Ferric ion hydr(oxo) clusters in the 'Venus-Fly-Trap' cleft of FbpA: Mössbauer, calorimetric and mass spectrometric studies

Arindam Mukherjee, Paul R. Bilton, Logan Mackay, Adam Janoschka, Haizhong Zhu, Dean Rea, Pat R.R. Langridge-Smith, Dominic J. Campopiano, Thomas Teschner, Alfred X. Trautwein, Volker Schünemann, Peter J. Sadler

A. Mukherjee

Department of Chemical Sciences

Indian Institute of Science Education and Research Kolkata

Mohnapur campus, Nadia-741252, India

Tel.: +91-33–25873121 (Extn-242)

Fax: +91-33-25873020

Former address: Department of Chemistry, University of Warwick

P. J. Sadler(✉) · D. Rea

Department of Chemistry

University of Warwick

Coventry, CV4 7AL

United Kingdom

Tel: +44 (0)24 76523818; Fax: +44 (0)24 76523819

e-mail: p.j.sadler@warwick.ac.uk

P. R. Bilton ·H. Zhu, ·D. J. Campopiano

School of Chemistry

University of Edinburgh

Edinburgh, EH9 3JJ

United Kingdom

L. MacKay • P. R. R. Langridge-Smith

SIRCAMS, School of Chemistry

University of Edinburgh

Edinburgh, EH93JJ

United Kingdom

A. Janoschka ·V. Schünemann,

University of Kaiserslautern

Erwin-Schrödinger-Straße Gebäude 56

67663 Kaiserslautern

Germany

Tel.: +49(0)631 205 4920; Fax: +49(0)631 205 4958

T. Teschner ·A.X. Trautwein,

University of Lübeck

Ratzeburger Allee 160a

23538 Lübeck

Germany

Tel.: +49(0)451 500 4204; Fax: +49(0)451 500 4214

Abstract

Isothermal calorimetric studies of the binding of iron(III) citrate to ferric ion binding protein (FbpA) from *Neisseria gonorrhoeae* suggested complexation of a tetranuclear iron(III) cluster as a single step binding event (binding constant K = 6.0(5) x 10^5 M^{-1}). High resolution Fourier transform ion cyclotron resonance (FTICR) mass spectrometric data supported the binding of a tetranuclear oxo(hydroxo) iron(III) cluster of formula $[Fe_4O_2(OH)_4(H_2O)(cit)]^+$ in the interdomain binding cleft of FbpA. The mutant H9Y-*n*FbpA showed a two fold increase in the apparent binding constant [K_{app}^{ITC} = 1.1(7) x 10^6 M^{-1}] for the tetranuclear iron(III) cluster compared to the wild-type protein. Mössbauer spectra of FbpA from *E. coli* cells cultured in the presence of added ^{57}Fe-citrate were indicative of the presence of dinuclear and polynuclear clusters. FbpA therefore appears to have a strong affinity for iron clusters in iron-rich environments, a property which might endow the protein with new biological functions.

Keywords Ferric-ion binding Protein A ·Bacterial transferrin ·Isothermal titration calorimetry ·Iron clusters ·Fourier transform mass spectrometry ·Mössbauer spectroscopy

Abbreviations

ITC	Isothermal titration calorimetry
FbpA	Ferric ion binding protein A
FbpB	Ferric ion binding protein B
FbpC	Ferric ion binding protein C
PhoU	Phosphate transport system protein
*n*FbpA	Ferric ion binding protein A from *Neisseria gonorrhoeae*
*h*FbpA	Ferric ion binding protein A from *Haemophilus influenzae*
ESI-MS	Electrospray ionization mass spectrometry
FTICR	Fourier transform ion cyclotron resonance
ICPMS	Inductively coupled plasma mass spectrometry

Introduction

Iron is required to increase the virulence of certain pathogenic strains [1]. In the oxidizing atmosphere of earth, iron is mostly present as Fe^{III} which has restricted its aqueous solubility. Fe^{III}-binding proteins are therefore of high importance for their ability to solubilise and transport Fe^{III} [2]. Some pathogens use FbpA (ferric ion binding protein A) to sequester Fe^{III} in a soluble form in the periplasm and deliver it to the cytoplasm via formation of an ABC transporter complex of FbpA, FbpB (transmembrane protein) and FbpC (ATPase) in the inner cell membrane [3].

FbpA is a member of the transferrin family of proteins which includes serum transferrin and lactoferrin. These proteins bind a single Fe^{III} tightly in an interdomain cleft ('Venus Fly-Trap') with ligands not only from protein side chains, including two tyrosines, but also from a synergistic anion - carbonate in the case of serum transferrin and lactoferrin, and phosphate in the case of FbpA [4,5]. Whereas transferrin and lactoferrin are bi-lobal and can bind two Fe^{III} ions, one in each lobe, bacterial FbpA is monolobal. The iron binding site is shown in Fig. 1.

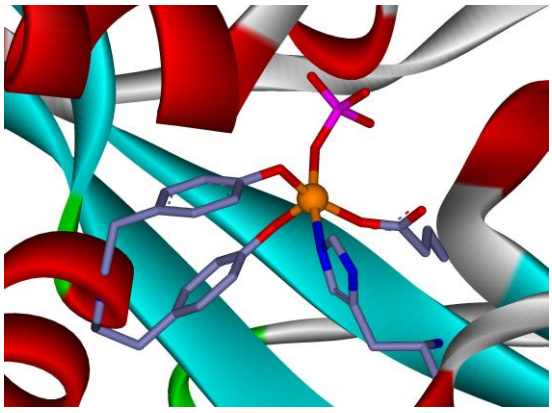

Fig. 1 The active site of *n*FbpA showing the two tyrosines (Y195 and Y196, *left*), histidine (H9, *bottom*), glutamate (E57, *right*), and phosphate (synergistic anion, *top*) as Fe^{III} (*orange ball*) ligands (PDB 1D9Y).

Although most thoroughly characterized as a single Fe^{III}-transporting periplasmic protein, FbpA can bind polynuclear (hydr)oxo metal species [6-8]. Two X-ray crystal structures have been reported which contain a Fe^{III}_3-(hydr)oxo cluster in *n*FbpA (FbpA from *Neisseria Gonorrhoeae*) [9], and a Fe^{III}_4-oxo cluster in the active site of a mutant of *h*FbpA from *Haemophilus influenza* [10]. Such clusters may confer other properties on FbpA which might have biological importance, e.g. phosphatase activity [9]. However, no detailed studies have been performed in order to investigate the binding of Fe^{III}_3- and Fe^{III}_4-clusters in solution and the thermodynamics of the process. It is therefore of interest to determine the stoichiometry of multiple iron binding to *n*FbpA in order to gain insight into the binding energetics and its possible role in metal homeostasis, detoxification and bio-mineralization of Fe^{III}.

In general, proteins having non-heme polynuclear iron sites play important roles in a plethora of important physiological reactions including oxygen transport, oxygenases and hydrogenases [11-17]. Recently it has been shown that a phosphate uptake and transfer protein (PhoU) homologue from *Thermatoga maritima* found in geothermal-heated marine sediments contains phosphate and carboxylato bound multinuclear iron(III) centers [14]. FbpA may also play a role in phosphate ester hydrolysis in its native and Fe_3-loaded forms [18,19].

Although in the majority bacterial FbpA homologues the Fe^{III} binds to two tyrosines, a histidine and a glutamate along with a phosphate as the synergistic anion (Fig.1), in certain species such as *Pasteurella Haemolytica*, the FbpA uses three tyrosine and one aspartate side-chain to coordinate the metal (Table 1). This interesting difference has led us to investigate the change in iron affinity upon introduction of a third Tyr in place of a His residue, as a ligand for Fe^{III} in *n*FbpA.

We report studies of the binding of polynuclear (hydr)oxo iron species to *n*FbpA and the mutant H9Y-*n*FbpA using isothermal titration calorimetry, inductively coupled plasma- mass

spectrometry, Fourier transform ion cyclotron-electrospray ionisation (FTICR-ESI) mass spectrometry, and Mössbauer spectroscopy.

Table 1. Some reported native and metal-site mutant ferric ion binding proteins.

Protein	**Source Organism**	**Metal site**[#]	**Pdb code**[Ref]
*n*FbpA	*Neisseria gonorrhoeae*	**H9**, **E57**, **Y195**, **Y196**, Fe and **PO_4^{3-}**	1D9Y [20]
Hf_5- and Hf_3-*n*FbpA	*Neisseria gonorrhoeae*	H9, E57, **Y195**, **Y196** Hf_5 , Hf_3, **μ_3-oxygen**, **μ_2-oxygen**, **PO_4^{3-}**	1O7T [21]
Zr_3-*n*FbpA	*Neisseria gonorrhoeae*	H9, E57, **Y195**, **Y196**, Zr_3 and **PO_4^{3-}**	1XC1 [22]
Y195I-*n*FbpA*	*Neisseria gonorrhoeae*	H9, E57, I195, Y196 - *mutation has major effect on iron binding*	[23]
Fe_3-*n*FbpA	*Neisseria gonorrhoeae*	H9, E57, **Y195**, **Y196** Fe_3 , **μ_3-oxygen**, **μ_2-oxygen**, **PO_4^{3-}**	1R1N [9]
Q58E-, Q58R-, and G140H-*n*FbpA*	*Neisseria gonorrhoeae*	H9, E57, Y195, Y196	[24]
*Mh*FbpA	*Mannheimia haemolytica*	**Y142**, **Y198**, **Y199**, **carbonate** and Fe **Y142**, **Y198**, **Y199**, and Fe	1SI0 [25] 1SI1 [25]
Apo-*Ph*FbpA	*Pasteurella haemolytica*	Y142, E11, Y198, Y199, formate x 2	1Q35 [26]
*Y*fuA Apo-*Y*fuA	*Yersinia enterocolitica*	**H14**, **E62**, **D144**, **Y198**, **Y199**, Fe H14, E62, D144, Y198, Y199, citrate	1XVX[27] 1XVY[27]

*c*FbpA	*Campylobacter jejuni*	**H14**, **Y15**, **Y146**, **Y202**, **Y203**, Fe	1Y4T [28]
*b*FbpA	*Bordetella pertussis*	Y143, Y199, Y200 **Y143**, Y199, **Y200**, Fe, **$(C_2H_2O_4)_2$** **Y143**, **Y199**, **Y200**, Fe, **carbonate**	1Y9U [28] 2OWS[29] 2OWT[29]
Apo-*h*FbpA	*Haemophilus Influenzae*	H9, E57, Y195, Y196	1D9V [30]
*h*FbpA	*Haemophilus influenzae*	**H9**, **E57**, **Y195**, **Y196**, Fe and **PO_4^{3-}**	1MRP [31]
H9Q- *h*FbpA	*Haemophilus influenzae*	Q9, **Y195**, **Y196**, Fe and **EDTA**	1NNF [32]
N175L-*h*FbpA	*Haemophilus influenzae*	H9, E57, **Y195**, **Y196**, Fe_4 and **PO_4^{3-}**	1QW0[10]
H9A-*h*FbpA	*Haemophilus influenzae*	A9, E57, **Y195**, **Y196**, Fe_3 and **$(PO_4^{3-})_2$**	1QVS [10]
Q58L-*h*FbpA	*Haemophilus influenza*	H9, E57, **Y195**, **Y196**, Fe and **PO_4^{3-}**	2O68 [33]
N193L-*h*FbpA	*Haemophilus influenza*	H9, E57, **Y195**, **Y196** and Fe	2O69 [10]
E57A-*h*FbpA	*Haemophilus influenza*	H9, A57, **Y195**, **Y196**, Fe and **PO_4^{3-}**	2O6A [34]
H9A-, Y195A-, and Y196A-*h*FbpA*	*Haemophilus influenza*	*mutations have major effect on iron binding*	[34]

[#] *residues in bold are involved in coordination to metal*

**Structure not reported*

Materials and Methods

Citric acid, triammonium citrate (Sigma), $NaHCO_3$ (Aldrich), Hepes (Aldrich), Tris-HCl (Aldrich), cetyltrimethylammonium bromide (CTAB, Aldrich), ferric chloride hexahydrate and ferric ammonium citrate (Aldrich) were used as received. Iron and sulfur atomic absorption standard solutions were purchased from Aldrich. Citric acid tri-sodium salt was purchased from Fisher. The molecular-weight-cut-off (*mwco*) filters were purchased from Sartorius and Millipore. All other chemicals were reagent grade.

$^{57}FeCl_3$ solution was prepared using a modified literature procedure [35]. 0.0146 g ^{57}Fe (99.8% purity) was dissolved in 1 mL 37% HCl (over 2 d) and the solution was exposed in air and light until the color turned to brown-yellow. This solution was used for preparing ^{57}Fe-citrate complexes.

$^{57}FeCl_3$–Tris solution was made by dissolving 8 mg $^{57}Fe_2O_3$ in 1 mL 6 M HCl at 323 K over a period of 24 h, and then the solution was evaporated to dryness in a rotary evaporator and added 4.5 mL deionized water. To the above solution solid Tris base was added to adjust the pH to 7.4. The final concentration was adjusted to 10 mM and stored in a refrigerator until further use. This solution was used for binding ^{57}Fe to apo-H9Y-*n*FbpA in FTICR-ESI mass spectrometry methods. To study iron binding to apo-*n*FbpA and apo-H9Y-*n*FbpA by FTICR-ESI mass spectrometry ferric ammonium citrate in Tris buffer pH7.4 was used.

$[Fe^{III}(cit)_2]^{5-}$ of the required molarity was synthesized using literature procedure [36] and then a 4 mM solution was made in the same buffer used to prepare the apo-*n*FbpA solution (viz. 50 mM Tris buffer pH 7.45). Stock solutions of ferric ammonium citrate were prepared in the same buffer used to prepare apo-*n*FbpA stock solution. All buffer solutions were passed through Chelex resin (Aldrich) prior to use. This iron solution was used in ITC method for iron uptake by *n*FbpA.

The ^{57}Fe-citrate-complex was prepared by mixing $^{57}FeCl_3$ solution and Na_3Hcit solution in equimolar quantities and adjusting the pH to 5.8 with NaOH. The freshly prepared dark-green ^{57}Fe-citrate was divided into two aliquots. One was diluted with water to a concentration of 2.58 mM and stored in dark in refrigerator. The other aliquot was exposed to light and air until the color turned to brown-red. This aged ^{57}Fe-citrate solution was diluted with water (concentration 2.58 mM) and stored at 253 K until required). These solutions were used for Mössbauer spectroscopic studies. The aged ^{57}Fe-citrate solution was also used for the preparation of ^{57}Fe bound *n*FbpA sample used in Mössbauer spectroscopic studies. All enrichment reactions were carried out in apparatus washed with 3M HCl and deionised water prior to use. The buffer solutions and water used were passed through Chelex resin to ensure they were free of iron.

Cloning and Protein Expression

The FbpA gene from *Neisseria gonorrhoeae*, *n*FbpA, was subcloned into the plasmid pTRC 99A and used for cloning and expression [35]. Overexpression and purification of *n*FbpA *(Neisseria Gonorrhoeae)* was performed by a literature method [37].

In order to introduce the single mutation of histidine-9 to tyrosine-9 the pTRC 99A-FbpA plasmid was used as a template using the following primers:

forward primer 5'-TACAACGGCCAA<u>TAC</u>AAAGAAGCG-3'

reverse primer 5'-CGCTTCTTT<u>GTA</u>TTGGCCGTTGTA-3'

to introduce the single mutation of histidine-9 to tyrosine-9. The mutated codon is underlined in the primer sequences shown. The mutant genes were completely characterized by DNA sequencing prior to expression in *Escherichia coli* TOP 10 cells. The expression and purification were carried out using literature procedures [35]. The molar extinction coefficient ε_{280} of the pure protein was calculated as 50,390 M^{-1} cm^{-1} by addition of 1490 M^{-1} cm^{-1} for the inclusion of a

tyrosine to the experimental absorption coefficient (ε_{280} = 48,900 M^{-1} cm^{-1}) of native holo-*n*FbpA [38,39].

Preparation of apo-*n*FbpA and apo-H9Y-*n*FbpA

Apo-*n*FbpA and apo-H9Y-*n*FbpA were prepared by treatment of the respective holo-protein solutions in a 10 kDa *mwco* centrifugal filter (Amicon) with 100 mM sodium citrate (pH 6.0) until there was negligible absorbance at 480 nm. The apo-*n*FbpA was then dialyzed extensively with 50 mM Tris-HCl buffer pH 7.45 ± 0.05. The final protein and buffer solutions (used in dialysis) were passed through Millipore 0.2 μm sterile filters prior to their use in ITC experiments. The concentrations of apo-*n*FbpA and apo-H9Y-*n*FbpA were determined from the absorbance at 280 nm (ε_{280} = 44,300 M^{-1} cm^{-1} apo-*n*FbpA and ε_{280} = 45,800 M^{-1} cm^{-1} apo-H9Y-*n*FbpA).

Preparation of ^{57}Fe-enriched *E. coli* cells.

Normal LB medium was prepared and sterilized; then aged ^{57}Fe-cit solution was sterile-filtered into the medium such that the final concentration of ^{57}Fe-cit was ~30 μM (the original ^{56}Fe concentration in LB medium was 6.5 μM, analyzed by ICP-MS). TOP 10 strains (Invitrogen), containing the plasmid pTrc99A/FbpA/Ng to over-express *n*FbpA were grown at 37 ˚C for 16 h in the LB medium enriched with 30 μM aged ^{57}Fe-citrate-complex. As a control, TOP 10 strains without pTrc99A/FbpA/Ng plasmid were grown under the same conditions except no antibiotics were added. Cells were harvested by centrifugation at 4 ˚C. Wet-packed cells of TOP 10 / *n*FbpA and TOP 10 were then transferred separately to 1 mL Mössbauer sample holders and frozen in liquid nitrogen. Wet-packed cells of TOP 10 / *n*FbpA were also transferred to an EPR tube.

TOP 10 cells containing pTrc99A/FbpA/Ng plasmid grown using the above method were used to extract the $^{57}Fe_n$-*n*FbpA which was purified according to a literature method [40]. This sample was used as a source of the $^{57}Fe_n$-*n*FbpA sample for Mössbauer spectroscopy and EPR. However the Mössbauer results indicate that in fact the mono-ferric protein ^{57}Fe-*n*FbpA was extracted (see Discussion).

Preparation of reloaded $^{57}Fe_n$-*n*FbpA

Apo-H9Y-*n*FbpA was reloaded with ^{57}Fe without citrate by using a ^{57}Fe-Tris solution as described below. A 25 µL aliquot of 10 mM $^{57}FeCl_3$-Tris solution was added to 300 µL of 80 µM apo-H9Y-*n*FbpA and incubated at 298 K for 8 h. Any low molecular weight substances were removed using a PD-10 column followed by centrifugation with a 10 kDa *mwco* centrifugal filter. The above ^{57}Fe reloaded H9Y-*n*FbpA sample was used for FTICR mass spectrometry.

Isothermal Titration Calorimetry (ITC)

The isothermal titration calorimetry studies of reactions of apo-*n*FbpA with ferric ammonium citrate and $[Fe^{III}(cit)_2]^{5-}$ were carried out on a MicroCal VP-ITC (MicroCal Inc., Northampton, MA) having a cell volume of 1.4537 mL using a stirring speed of 286 rpm. Data acquisition and analysis were performed using software (Origin) supplied by MicroCal. Titrations were performed in 50 mM Tris-HCl, pH 7.4 or 50 mM Hepes buffer pH 7.4 at 298 K. For each titration a 2-8 µL aliquots of 4-10 mM ferric ammonium citrate or 4 mM $[Fe^{III}(cit)_2]^{5-}$ were injected into the sample cell containing 66-100 µM apo-*n*FbpA or apo-H9Y-*n*FbpA. The time between each injection was selected based on the equilibration time dependence of the binding reactions. Control experiments were performed to account for the heat of dilution of citrate, $[Fe^{III}(cit)_2]^{5-}$, ferric ammonium citrate and the binding of citrate to *n*FbpA using the same

experimental conditions as the *n*FbpA metal binding experiments. The heats for the control experiments were subtracted from the heat generated during the titration of metal citrates with protein. For experiments in the presence of citrate bound to *n*FbpA prior to metal binding, the citrate was added to *n*FbpA 24 h before the titrations and equilibrated at 298 K.

ESI mass spectrometric studies

FTICR electrospray mass spectrometry was performed on a Bruker 12 Tesla FTICR-ESI mass spectrometer equipped with an UltiMate 3000 series system (Dionex, UK) with nanoflow splitter, coupled to the mass spectrometer using a TriVersa NanoMate (Advion, Ithaca, NY) with an electrospray potential of 1.7 kV. All spectra were acquired using Bruker Daltonics software with 512 k data points in the range 2200–3600 *m/z*.

ESI mass spectrometric studies of the ITC samples were carried out using a Bruker microTOF platform. Bruker Daltonics Data Analysis software was used for all the data analysis and post processing. The Fe_4-*n*FbpA samples obtained as a result of the ITC experiments were exchanged with 0.05 M NaCl using a 10 kDa mwco centrifugal filter and concentrated to a small volume of ~200 µL. The concentration of the solution was determined from the absorption at 280 nm. The final concentration was adjusted to 10 µM in a 100 mM ammonium acetate solution of pH 7.45 (pH adjusted with 5 M aqueous ammonia solution).

The iron(III)-bound sample of wild-type *n*FbpA for FTICR mass spectrometry was prepared by addition of 30 µL of 10 mM ferric ammonium citrate to 300 µL of 80 µM apo-*n*FbpA in Tris buffer pH 7.45 and incubated at 298 K for 12 h. The metal-bound protein was separated from unbound metal using a PD-10 de-salting column pre-equilibrated with HPLC grade water. The concentration of the sample was then determined from the absorbance at 280 nm. The final concentration of the sample used for nanospray MS was 15 µM Fe_4-*n*FbpA.

The H9Y-*n*FbpA-^{57}Fe complex for FTICR mass spectrometry was prepared by adding ammonium acetate solution and isopropanol to ^{57}Fe reloaded H9Y-*n*FbpA such that the final concentration of the sample for mass spectrometry was 15 µM $^{57}Fe_4$-H9Y-*n*FbpA in 20 mM ammonium acetate and 10% isopropanol.

Mössbauer Spectroscopy

Mössbauer spectra were recorded using a conventional spectrometer in the constant-acceleration mode. Isomer shifts are given relative to α-Fe at room temperature. The spectra obtained at 20 mT (perpendicular to the γ-beam) were measured in a bath cryostat (Oxford MD 306), equipped with a pair of permanent magnets. The spectra obtained at high fields were measured in a cryostat equipped with a superconducting magnet (Oxford Spectromag 4000M). A paramagnetic spin system with spin $\vec{S}$ in an external field $\vec{B}$ can be described by the following spin Hamiltonian including the zero field splitting D and the rhombicity parameter $\frac{E}{D}$:

$$\hat{H}_{fs} = D\left[\hat{S}_z^2 - \frac{1}{3}S(S+1) + \frac{E}{D}\left(\hat{S}_x^2 - \hat{S}_y^2\right)\right] + \mu_B \vec{S}\vec{g}\vec{B}.$$

The components of the spin operators are denoted by $\hat{S}_{x,y,z}$. $\vec{g}$ represents the electronic g-tensor and S the spin quantum number. In order to calculate magnetic Mössbauer spectra, spin expectation values $\langle\vec{S}\rangle_i$ for every eigenfunction ϕ_i of the electronic spin Hamiltonian given above have been calculated and subsequently used in order to simulate the experimentally observed magnetic Mössbauer spectra under different field conditions. For that purpose the following usual nuclear Hamiltonian was used:

$$\hat{H}_i = \frac{eQV_{zz}}{4I(2I-1)}[3\hat{I}_z^2 - I(I+1) + \eta(\hat{I}_x^2 - \hat{I}_y^2)] - g_N\mu_N\vec{B}\vec{I} + \langle\vec{S}\rangle_i\vec{A}\vec{I}$$

Here I denotes the nuclear spin, Q is the nuclear quadrupole moment of the excited nuclear state of ^{57}Fe, V_{zz} is the main component of the electric-field gradient tensor, which gives rise to the quadrupole splitting and $\eta=(V_{xx} - V_{yy})/V_{zz}$ is the asymmetry parameter of the electric field gradient. $\vec{\vec{A}}$ denotes the hyperfine coupling tensor, g_N is the nuclear g-factor, μ_N is the nuclear

magneton and $\vec{B}$ is the applied external field [41,42]. The simulated magnetic Mössbauer spectra presented in this study have all been performed in the slow relaxation limit, which means that the nuclear Hamiltonian $\hat{H}_i$ was diagonalized for every spin expectation values $\langle \vec{S} \rangle_i$ separately (for details see [41]). Non magnetic Mössbauer spectra were analyzed by least-square fits using Lorentzian line shapes.

Inductively coupled plasma mass spectrometry (ICP-MS)

Protein samples of the purified metal-protein complexes for ICP-MS were prepared by making dilutions in 5 mM NH_4OAc. Elemental analysis was carried out on a quadrupole ICP-MS model 7500ce, Agilent Technologies, Tokyo, Japan. The instrument consists of an ICP source with plasma-shield torch, an enclosed octapole ion guide operated in the RF mode and a quadrupole mass analyser with a SEM detector. Two iron isotopes (^{56}Fe and ^{57}Fe) and sulfur (^{32}S) were monitored by ICP-MS. A standard calibration curve was prepared using seven different dilutions (0, 50, 100, 200, 400, 800, 1600 ppb) of Aldrich certified standards for iron and sulfur in 3% v/v ultra pure nitric acid. A solution of 3% v/v ultra pure nitric acid in de-ionized water was also used to check the background level caused by polyatomic Ar interferences. Xenon was used as the collision gas to minimize interferences in S measurements. Erbium (^{166}Er) was used as internal standard for all the measurements.

Results

The ferric ion binding protein, *n*FbpA, is known to bind to Fe^{III} ions via the side chains of H9, E57, Y195 and Y196 in the 'Venus-fly-trap' cleft of the protein, together with binding to a synergistic anion (e.g. phosphate, nitrilotriacetate, sulfate). Our present investigation involves the study of multiple iron(III) binding to apo-*n*FbpA using iron citrates as the metal source. Based on a wild-type variant of FbpA isolated from *Bordetella pertussis,* [28,29] we have also studied the

mutant protein H9Y-*n*FbpA *(Neisseria gonorrhoeae)* in which histidine-9 is replaced by tyrosine, so providing three tyrosines and a glutamate for possible Fe^{III} binding at the active site. All our experiments were carried out in the absence of added phosphate in order to avoid possible complications in the heat of reaction studies due to competition between citrate and phosphate as synergistic anions and to avoid precipitation of any insoluble Fe^{III} phosphate during ITC titrations.

Isothermal titration calorimetry

Isothermal titration calorimetry of a 80-100 μM solution of *n*FbpA in 50 mM Tris-HCl buffer with or without pre-equilibration with citrate at pH 7.45 at 298 K shows binding of four Fe^{III} to

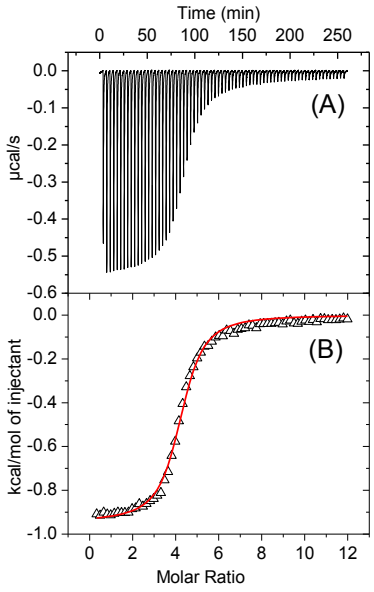

Fig. 2 (A) Raw ITC data, and (B) Corrected integrated heat of reaction fitted with a single-site binding model. Conditions: 80 μM apo-*n*FbpA in 50 mM Tris-HCl buffer pH 7.4 in the sample cell and the injectant of 10 mM ferric ammonium citrate in the same buffer. 2 μL injections were made with a delay time of 220 s between each injection.

apo-*n*FbpA and H9Y-*n*FbpA fitted using a single-site binding model. The theoretical fit of the data suggests either that four iron ions are bound to a single-site or that four iron atoms are bound to four identical sites, and that the binding reaction is exothermic.

An 80 μM apo-*n*FbpA solution in 50 mM Tris-HCl buffer at pH 7.4 was titrated against 10 mM ferric ammonium citrate using 70 injections of 2 μL each spaced 220 s apart. The results (Fig. 2) show that the metal binding to the protein overall is exothermic, exhibiting a single kinetic phase. During the initial phase of the binding isotherm almost all the injected iron citrate binds to the protein and after the 12th injection the heat evolved begins to decrease; saturation of iron binding appears to be achieved at about the 57th injection. Control experiments suggested that the heat evolved after the 57th injection is due to the interaction of ferric ammonium citrate with the Fe^{III}-saturated protein in solution. The binding was best modeled using the single-site binding model. The ITC data fitted well to a single site binding model, giving a binding constant, K_{app}^{ITC} = 6.0(5) x 10^5 M^{-1} with *N* (number of metal ions bound per protein molecule) value of 4.23(2) which signifies at least 4 Fe^{III} ions bound per protein molecule. The integrated heat of the binding reaction as determined for the single-site binding model is -0.95(5) kcal mol^{-1} (Table 2).

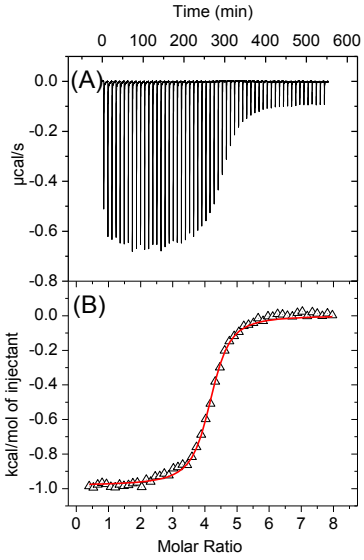

Fig. 3 (A) Raw ITC data, and (B) Corrected integrated heat of reaction fitted with a single-site binding model. Conditions: 100 μM apo-*n*FbpA in 50 mM Tris-HCl buffer pH 7.4 with 4 mM $[Fe(cit)_2]^{5-}$ in 50 mM Tris-HCl buffer pH 7.4 as the injectant. Each injection was 5 μL and the delay time between injections was 600 s.

In another experiment, we used a solution of an iron citrate complex which contains two molar equivalents of citrate per mole of Fe^{III}. A 4 mM $[Fe(cit)_2]^{5-}$ was used as the injectant and titrated with 100 µM apo-*n*FbpA in the sample cell at 298 K. A total of 55 injections were made, each of 5 µL at a spacing of 600 s. In this case, although the overall reaction was exothermic as expected, the initial phase of the binding isotherm during the first 8 injections was more exothermic and began to reach a plateau after about the 17^{th} injection. After the 26^{th} injection the onset of protein saturation was observed. The heat evolved began to decrease and saturation was

Table 2 Binding constants and the enthalpy changes for binding of Fe^{III} to apo-*n*FbpA as determined from ITC data based on a single-site model.

Protein solution	Titrant[#]	K_{app}^{ITC} (M^{-1})	ΔH (kcal mol^{-1})	N[‡]
in Tris-HCl buffer pH 7.4				
80 µM apo-*n*FbpA	10 mM fac	6.0(5) x 10^5	-0.95(5)	4.23(2)
100 µM apo-*n*FbpA	4 mM $[Fe(cit)_2]^{5-}$	4.6(7) x 10^5	-0.96(3)	4.28(2)
100 µM apo-*n*FbpA[§]	4 mM fac	7.6(8) x 10^4	-0.87(5)	4.36(2)
80 µM apo-H9Y-*n*FbpA	10 mM fac	1.1(7) x 10^6	-1.03(6)	4.06(2)
in Hepes buffer pH 7.4				
76 µM apo-*n*FbpA	4 mM fac	8.4(6) x 10^4	-0.30(7)	4.26(4)
66 µM apo-H9Y-*n*FbpA	5 mM fac	4.5(5) x 10^5	-0.48(5)	4.18(3)

[#] fac = Ferric ammonium citrate; [‡] N = reaction stoichiometry number (no. of metal ions per protein molecule); [§] apo-*n*FbpA was pre-equilibrated with 4 mM citrate for 24 h

achieved at ca. the 45^{th} injection (Fig. 3). The binding was best modeled using the single-site binding model giving a binding constant of 4.6(7) x 10^5 M^{-1} and a corrected integrated heat of binding of -0.96(3) kcal mol^{-1} (Table 2). The N value from the best fit was 4.28(2) which suggests that at least 4 Fe^{III} ions are bound per protein molecule.

ITC experiments were also carried out using 100 μM apo-*n*FbpA pre-equilibrated with 4 mM citrate in Tris-HCl buffer pH 7.4 in the sample cell at 298 K with 4 mM ferric ammonium citrate as injectant. The 5 μL injections were spaced at 600 s and in total 55 aliquots were injected. The best theoretical fit was achieved using the single-site binding model, and the fitting

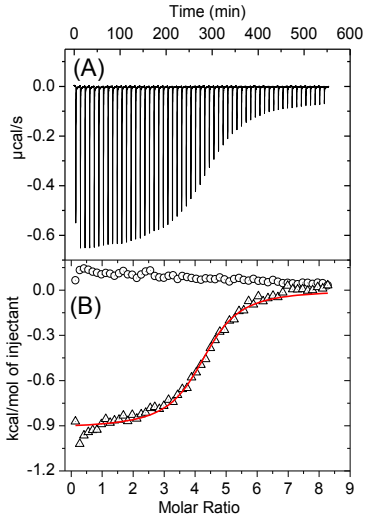

Fig. 4 Calorimetric titrations showing raw isothermal titration data (A) for 5 μL injections at an interval of 10 min, of 4 mM ferric ammonium citrate in to 100 μM apo-*n*FbpA pre-equilibrated with 4 mM citrate, both the metal complex and the protein solution were in 50 mM Tris-HCl buffer pH 7.4. (B) Corrected integrated heat of reaction (Δ) of the metal-protein adduct fitted using a single-site binding model and the integrated heat of reaction (o) for the titration of ferric ammonium citrate in 4 mM citrate pre-equilibrated 50 mM Tris-HCl buffer pH 7.4.

gave an *N* value of 4.36(2), suggesting that at least four Fe^{III} ions bind per protein molecule (Fig. 4). However the binding constant (7.6(8) x 10^4 M^{-1}) is almost an order of magnitude less than when citrate was not pre-equilibrated with apo-*n*FbpA (6.0(5) x 10^5 M^{-1}, Table 2). Initial injections reflect a slope associated with an exothermic event which is almost finished by the 10^{th} injection. After this the detected heat change from individual injections reaches almost a constant until the 19^{th} injection, after which it begins to decrease, suggesting that the binding sites start to become saturated with iron. By the 50^{th} injection, all the protein molecules are saturated.

An ITC experiment was carried out with the mutant apo-H9Y-*n*FbpA in order to determine the influence of replacement of histidine by tyrosine in the Fe^{III} binding site. This provides the active site with three potential phenolates from three tyrosines and a glutamate carboxyl group for coordination to Fe^{III}. The binding experiments were performed using 80 µM apo-H9Y-*n*FbpA solution in 50 mM Tris-HCl buffer at pH 7.4 in the sample cell titrated with 10 mM ferric ammonium citrate as the injectant. A total of thirty 3.5 µL injections were made at intervals of 450 s at 298 K (Fig. 5). Iron(III) binding to apo-H9Y-*n*FbpA was relatively more exothermic than for the wild-type protein. The binding isotherm shows that the ability of the protein to bind four iron(III) ions decreases sharply after the 12^{th} injection and most of the protein molecules are

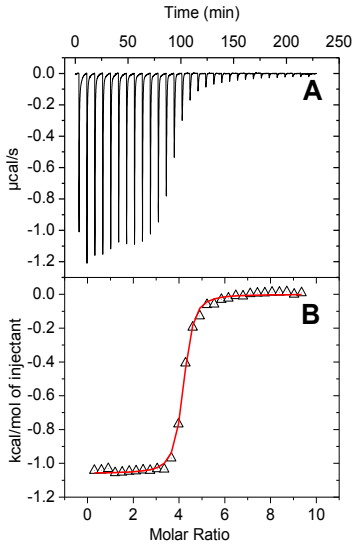

Fig. 5 Raw ITC data (A) and (B) integrated heat of reaction fitted with a single-site binding model. Conditions: 80 µM *apo*-H9Y-*n*FbpA in 50 mM Tris-HCl buffer pH 7.4 with 10 mM ferric ammonium citrate in 50 mM Tris-HCl buffer pH 7.4 as the injectant. Each injection was 3.5 µL and the delay time between each injection was 450 s.

saturated after the 22^{nd} injection (Fig. 5). The best theoretical fit using a single-site binding model gives an integrated heat of reaction of -1.03(6) kcal mol^{-1} which is similar to that for wild type *n*FbpA (ΔH of -0.95(5) kcal mol^{-1}) but with ca. 2x higher binding constant of 1.1(7) x 10^6

M^{-1} (vs. 6.0(5) x 10^5 M^{-1}, Table 2). The *N* value of 4.06(2) shows that at least four Fe^{III} ions are bound per protein molecule which is similar to the value obtained for the wild type *n*FbpA.

Calorimetric titrations of wild type apo-*n*FbpA and apo-H9Y-*n*FbpA were also carried out in 50 mM Hepes buffer at pH 7.4. A solution containing 76 μM wild type apo-*n*FbpA was titrated with 5 μL-injections of 4 mM ferric ammonium citrate spaced 480 s apart. The stoichiometry of iron binding determined by the best fit was N = 4.26(4) with the K_{app}^{ITC} = 8.4(6) x 10^4 M^{-1} and ΔH = -0.30(7) kcal mol^{-1} (Fig. S1). A solution containing 66 μM apo-H9Y-*n*Fbpa was titrated with 5 mM ferric ammonium citrate using 6 μL injections with a delay of 480 s between injections. The best fit gave a *N* value of 4.18(3) for the single-site binding model again which suggests the binding of at least four Fe^{III} per protein (Fig. S2). The binding constant K_{app}^{ITC} obtained is 4.5(5) x 10^5 M^{-1} and ΔH = -0.48(5) kcal mol^{-1}.

Mass spectrometry

To determine the protein metal ion stoichiometry of the iron-bound *n*FbpA samples, mass spectrometric experiments were carried out using Bruker microTOF and FTICR mass spectrometers. The ITC sample of *n*FbpA resulting from the titration with 10 mM ferric ammomium citrate (Fig. 2) was concentrated in 0.05 M NaCl and passed through a PD-10 column pre-equilibrated with deionized water. The concentration of the sample was then adjusted to 15 μM protein in 10 mM ammonium acetate containing 10% isopropanol. The microTOF mass spectrum revealed a peak at an m/z value of 2865.60 (where z = 12), deconvolution of which gives a mass of 34375.2 Da (Fig. S3). In addition peaks assignable to the apo-protein (obs. m/z = 33640.8 Da; calc m/z = 33638 Da) were present in the spectrum.

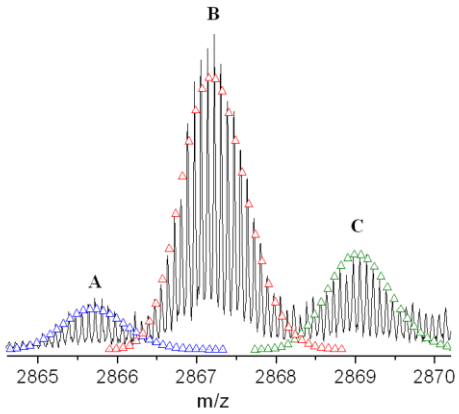

Fig. 6 FTICR-ESI mass spectrum of iron citrate bound wild-type *n*FbpA sample containing peaks assignable to Fe_4-*n*FbpA. The deconvolution of peak A gives a mass of 34375.62 Da (expt) which matches well with {apo-Fbp($C_{1508}H_{2415}N_{423}O_{446}S_1$) + $Fe_4O(OH)_5(cit)^{4-}$ + $(Hcit)^{3-}$ + $2(NH_4^+)$ +$12H^+$} (calc. 34375.86 Da); The deconvolution of peak B gives a mass of 34393.64 Da (expt) which matches well with {apo-Fbp($C_{1508}H_{2415}N_{423}O_{446}S_1$) + $Fe_4O(OH)_5(H_2O)(cit)^{4-}$ + $(Hcit)^{3-}$ + $2(NH_4^+)$ +$12H^+$} (calc. 34393.88 Da); The deconvolution of peak C gives a mass of 34415.86 Da (expt) which matches well with {apo-Fbp($C_{1508}H_{2415}N_{423}O_{446}S_1$) + $Fe_4O_2(OH)_4(H_2O)(Hcit)^{3-}$ + $(Hcit)^{3-}$ + $2(NH_4^+)$ + $11H^+$ + Na^+} (calc. 34415.66 Da).

Further confirmation of the binding of a tetranuclear Fe^{III} cluster, was obtained using FTICR electrospray ionisation mass spectrometry using a nanomate robot. The *n*FbpA:iron complex remained intact in the gas phase. We focused on the *n*FbpA 12+ state, assuming the protein to be still folded and "native" at this relatively low charge. Consistent with the ITC sample studied using microTOF ESI MS (Fig. S3) we observed a m/z peak corresponding to a deconvoluted mass of 34375.6 Da (Fig. 6). In addition a deconvoluted mass of 34393.6 Da was observed as shown in Fig. 6. A good fit to the observed mass ion peaks is a protein complex with a tetranuclear iron oxo(hydroxo) cluster as depicted in Fig. S3 and Fig. 6.

The ESI microTOF mass spectrometric analysis of the Fe_4^{III}-H9Y-*n*FbpA sample from the ITC experiment prepared using 10 mM ferric ammonium citrate as titrant (Fig. 5) gave m/z values of 2871.25 and 2835.0 Da. The deconvolution of the spectrum gave masses of 34443.0 and 34008.0 Da. The latter being the most abundant species in the spectrum (Fig. S4).

To obtain more accurate masses, FTICR was again performed with ^{57}Fe isotope labelling. For this study, citrate was avoided as a synergistic anion to simplify the interpretation of the

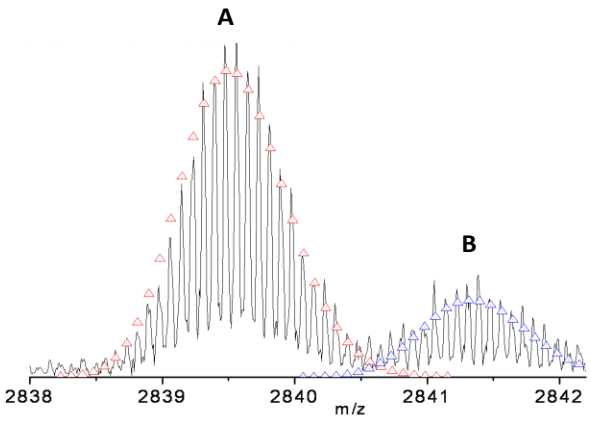

Fig. 7 FTICR-ESI mass spectrum of $^{57}Fe_4$-H9Y-*n*FbpA supporting the ITC data. The deconvolution of mass ion peak A gives a mass of 34062.67 Da (expt) which matches well with {apo-H9Y-*n*FbpA($C_{1511}H_{2417}N_{421}O_{447}S_1$) + $^{57}Fe_4O_2(OH)_4(H_2O)_3Na$ + $7H^+$}(calc. 34062.79 Da); The deconvolution of mass ion peak B gives a mass of 34084.62 Da (expt) which matches well with {apo-H9Y-*n*FbpA($C_{1511}H_{2417}N_{421}O_{447}S_1$) + $^{57}Fe_4O_2(OH)_4(H_2O)_3Na_2$ + $6H^+$} (calc. 34084.78 Da).

FTICR spectrum. Mass spectrometric data showed the 12+ charge state to be the most abundant ion (m/z, 2839.56) (Fig. 7), and deconvolution of the data gave an monoisotopic mass of 34062.7 Da, which is consistent with the formation of a tetranuclear iron(III) species.

Mössbauer spectroscopy

We have performed Mössbauer spectroscopy on both the freshly prepared as well of the aged ^{57}Fe citrate complex in order to compare it with the ^{57}Fe enriched *n*FbpA and *E. coli* cells. The Mössbauer spectrum of the fresh iron citrate-complex, Fig. S5a, was analyzed in terms of two species. Species I, with a relative contribution of 86 % to the total experimental area, exhibits an isomer shift of δ = 0.51 mm s^{-1} and a quadrupole splitting of ΔE_Q = 0.53 mm s^{-1}.

These parameters are typical of ferric high-spin iron. Species II (14% contribution) has δ = 1.39 mm s^{-1} and ΔE_Q = 3.21 mm s^{-1}, parameters typical of ferrous high-spin iron with a 6-fold (N/O)-coordination. The two-day-aged iron citrate-complex exhibits essentially the same components, except that the relative contribution of species II has increased to 34% (Fig. S5b). However, no signals for species I and II were detected in the Mössbauer spectra of *n*FbpA (Fig. S6) or from *E. coli* cells containing *n*FbpA and not-containing *n*FbpA (Figs. 8 and 9). In the cellular environment of *E. coli* in absence of *n*FbpA there are both ferrous and ferric high spin species. In case of *n*FbpA-expressing *E. coli* cells, with no *n*FbpA, polynuclear iron species ($^{57}Fe_n$ with n≥2) showing antiferromagnetic coupling are present, as indicated by analysis of the Mössbauer signals.

X-band EPR-measurements of ^{57}Fe-*n*FbpA show a broad anisotropic signal around g ≈ 4.3 which is indicative for a single ferric high-spin center with a rhombicity parameter *E/D* = 0.26 (not shown). The Mössbauer spectra of ^{57}Fe-*n*FbpA (Fig. S6) were analyzed by means of the spin-Hamiltonian formalism (solid lines in Fig. S6) and the following parameters have been obtained: *S* = 5/2, a zero-field splitting *D* = -0.65 cm^{-1}, *E/D* = 0.26, $A/g_N\mu_N$ = (-22.9, -22.4, -22.9) T, ΔE_Q = 0.12 mm s^{-1}, η = 0 and δ = 0.54 mm s^{-1} (Table 4).

Field dependent Mössbauer spectra of *E. coli* cells without *n*FbpA are shown in Fig. 8. X-band-EPR spectra show no signals characteristic for isolated half-integer spin systems. The spectrum taken at 4.2 K and 20 mT (Fig. 8a**)** was successfully simulated assuming 3 components: A doublet with δ = 1.25 ± 0.01 mm s^{-1}, ΔE_Q = 2.99 ± 0.01 mm s^{-1} and 33 % relative area (Table 3) can be assigned to high-spin ferrous iron in an octahedral coordination with N- and/or O-ligands. The remaining 66 % of the spectral area was analyzed by means of 2 components with a ratio of 1:1, which can be assigned to ferric ion sites with *S* = 5/2: The component Fe_1(III) exhibits δ =

0.47 ± 0.01 mm s^{-1} and ΔE_Q = 0.52 ± 0.01 mm s^{-1} and Fe_2(III) exhibits δ = 0.48 ± 0.01 mm s^{-1} and ΔE_Q = 1.15 ± 0.01 mm s^{-1}. Mössbauer spectra obtained in fields of 4 and 7 T show a more complex pattern (Fig. 8b and c). For the purpose of reproducing these strong-field spectra of *E. coli* cells phenomenologically, we have determined a set of spin-Hamiltonian parameters. This procedure is not appropriate for characterisation of different iron proteins (ferritin, heme iron proteins, non-heme iron proteins, iron-sulfur proteins in their specific oxidation states) in *E. coli* cells; it is, however, useful - together with the parameter set for *n*FbpA (from above) - for disentangling the Mössbauer spectra detected from *n*FbpA-expressing *E. coli* cells, described below (Figs. 9 and 10).

It should be mentioned that Top 10 *E. coli* cells have an iron citrate receptor, which is a protein in the outer membrane, so ferric citrate can still be taken up even without *n*FbpA production.

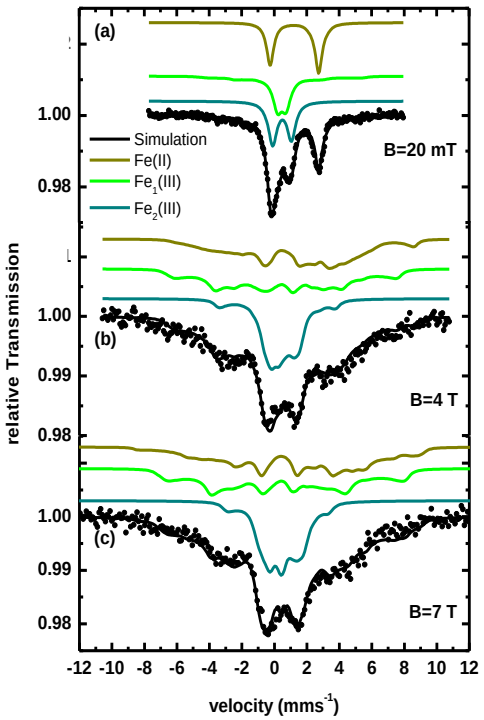

Fig. 8 Field dependent Mössbauer spectra of Top10 *E. coli* cells without *n*FbpA obtained at 4.2 K. The field was applied perpendicular to the γ-beam. The solid lines are spin-Hamiltonian simulations which have been performed in order to phenomenologically reproduce the experimental data assuming an artificial spin S = 3 (parameters see Table 3).

Fig. 9 shows a Mössbauer spectrum of ^{57}Fe enriched *n*FbpA-expressing Top 10 *E. coli* cells taken at 4.2 K in an applied field of 20 mT. In addition to the spectral pattern originating from Fe-*n*FbpA (30% relative area) and from Top 10 *E. coli* cells not expressing *n*FbpA (36% relative area), two other components can be identified. Component A with 7% relative area exhibits δ =

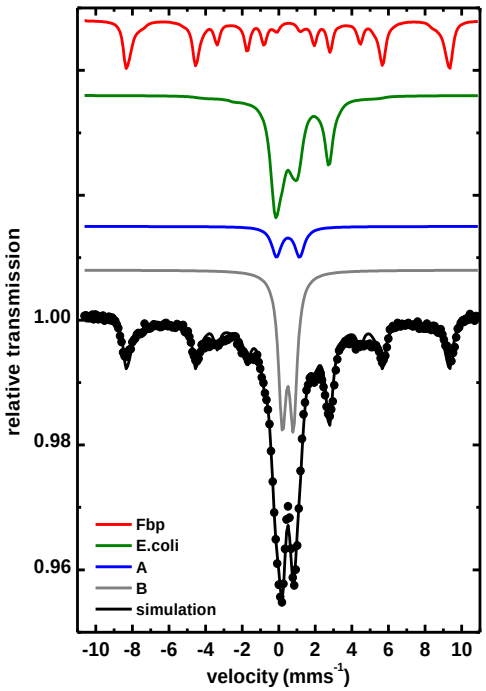

Fig. 9 Mössbauer spectrum of *n*FbpA-expressing Top 10 *E. coli* cells taken at T = 4.2 K in a 20 mT external field perpendicular to γ-beam. The solid lines are simulations: *n*FbpA (red), Top 10 *E .coli* cells without *n*FbpA (green), component A (blue) and B (gray) with parameters given in Table 4.

0.51 ± 0.01 mm s^{-1} and ΔE_Q = 1.26 ± 0.01 mm s^{-1}, and component B with 27% relative area has δ = 0.50 ± 0.01 mm s^{-1} and ΔE_Q = 0.60 ± 0.01 mm s^{-1}. Component A shows diamagnetic behavior in high magnetic fields (Fig. 10 and Table 4). Because δ ~ 0.5 mm s^{-1} is typical of ferric ions with spin S = 5/2, component A is representing a spin coupled system. Such behavior is typical of oxygen-bridged dimeric Fe^{III} centers as in methane monooxygenase [43] or ribonucleotide reductase [44]. Surprisingly component B splits in high magnetic fields into two subcomponents

B1 and B2 with a ratio of 1:1 (Fig. 10 and Table 4). Such behavior is typical of antiferromagnetically coupled oligomeric Fe_n^{III}-species [45]. Because B1 and B2 are in equal ratio it is tempting to postulate the presence of Fe_n^{III}-species with $n \geq 4$. The upper limit for n cannot be specified so the component B could also originate from a ferritin-like species.

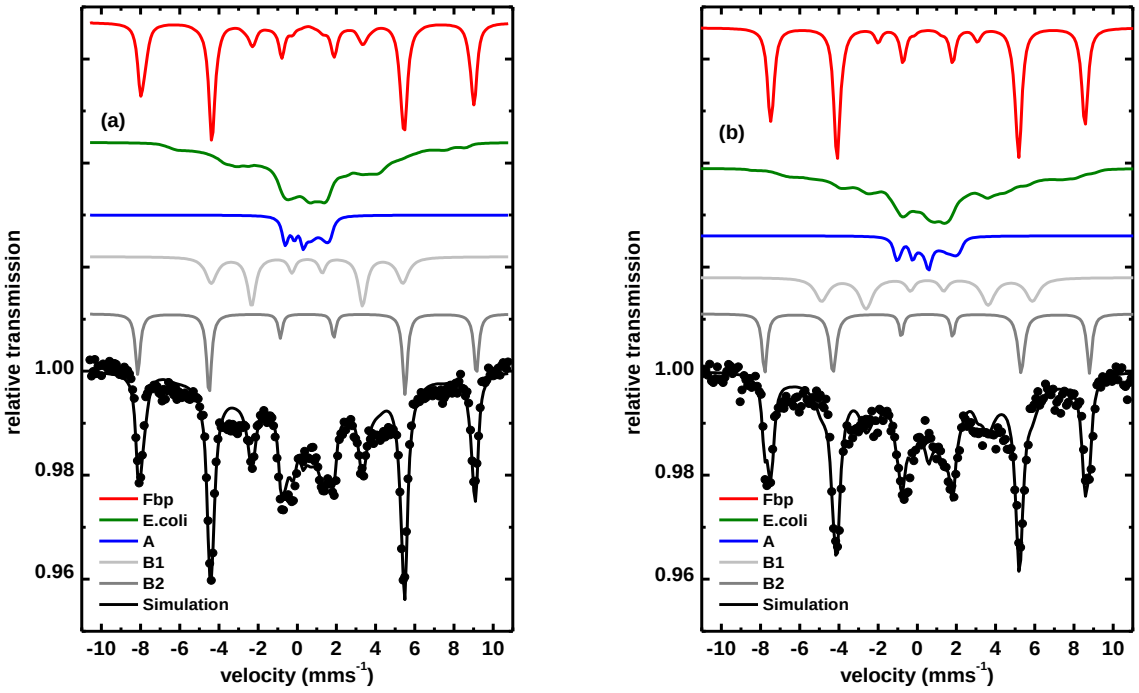

Fig. 10 Mössbauer spectra of *n*FbpA-expressing Top 10 *E. coli* cells taken at T = 4.2 K in external field of (a) 4 T and (b) 7 T perpendicular to the γ-beam. The solid lines are simulations with parameters given in Table 4. The red line represents *n*FbpA and the green line has been calculated with the parameters of the Top 10 *E. coli* cells not expressing FbpA given in Table 3.

Table 3 Mössbauer parameters from simulations of Mössbauer data (taken at 4.2 K and 20 mT) from *E. coli* cells without *n*FbpA.

E. coli	***S***	δ	ΔE_Q	***E/D***	***D***	η	β	B_{hf}	$A_{xx}/g_N\mu_N$	$A_{yy}/g_N\mu_N$	$A_{zz}/g_N\mu_N$	Γ	***Area***
		mm s^{-1}	**mm s^{-1}**		**cm^{-1}**			***T***	***T***	***T***	***T***	**mm s^{-1}**	**%**
Fe(II)	3	1.25	2.99	0.33	-0.79	1.0	0 °	-	3.4	-20.1	11.5	0.49	33
Fe_1(III)	3	0.47	-0.52	0.33	-0.08	1.0	90 °	-	-6.6	13.2	13.7	0.60	33
Fe_2(III)	3	0.48	-1.15	0.33	-0.74	1.0	30 °	-	0.6	-4	-8.9	0.60	33

Table 4 Mössbauer parameters from simulations of Mössbauer data from *E. coli* cells with *n*FbpA.

Sample	***S***	δ	ΔE_Q	***E/D***	***D***	η	β	B_{hf}	$A_{xx}/g_N\mu_N$	$A_{yy}/g_N\mu_N$	$A_{zz}/g_N\mu_N$	Γ	***Area***
		mm s^{-1}	**mm s^{-1}**		**cm^{-1}**			***T***	***T***	***T***	***T***	**mm s^{-1}**	**%**
*n*FbpA	5/2	0.54	0.12	0.26	-0.65	-	90 °	-	-22.9	-22.4	-22.9	0.35	30
E. coli						Parameters see Table 3							36
A	0	0.51	1.26			-		-				0.35	7
B (20 mT)		0.50	0.60									0.50	27
B1 (4 T)		0.50	0[a]					30				0.7; 0.5; 0.4	13.5
B1 (7T)		0.50	0					33				0.8;0.8;0.5	
B2 (4 T)		0.50	0[a]			--		53				0.3, 0.3; 0.25	13.5
B2 (7T)		0.50	0					51				0.3;0.4;0.25	

[a] The iron sites of polynuclear clusters may exhibit a random orientation of the main axis system of the electric field gradient tensor (V_{xx}, V_{yy}, V_{zz}) with respect to an applied external field. Therefore the observed quadrupole splitting ΔE_Q which is proportional to V_{zz} vanishes in this case.

Inductively coupled plasma mass spectrometry (ICP-MS)

The mass spectrometric samples were analysed by ICP-MS for total metal content. *n*FbpA contains one methionine sulphur, the only sulphur in the protein, hence determination of the iron-to-sulphur ratio gave a convenient and accurate determination of the iron-to-protein ratio. The samples were prepared by purifying and concentrating the metal-protein complex using 0.05 M NaCl and a 10 kDa *mwco* centrifugal filter, passing the sample through a PD-10 column, and finally diluting with 5 mM NH_4OAc to the required concentrations. This gave an Fe : S ratio of ca. 4.1(2):1. In contrast, when the sample from the ITC experiment with Tris buffer was washed with 20 mM NH_4OAc using a 10 kDa *mwco* centrifugal filter, the iron content decreased to 1.7(3) Fe per protein. Similarly, when the Fe-H9Y-*n*FbpA samples from the ITC experiments were concentrated and washed with 0.05 M NaCl using a 10 kDa *mwco* centrifugal filter, desalted using a PD-10 column, and exchanged into ammonium acetate as described above, the Fe:S ratio was found to be 3.9(3):1. When the latter sample was extensively dialyzed against 20 mM NH_4OAc, the iron-to-protein ratio decreased to 2.2(2):1.

Discussion

Isothermal titration calorimetry showed that the binding of Fe^{III} to *n*FbpA is exothermic at pH 7.4. The pH before and after the titrations remained constant (±0.05). The theoretical fit of the ITC data suggests that four iron atoms bind to a single-site on the protein, or the four iron atoms bind to four identical sites. Recent X-ray crystal structures have shown the presence of Fe^{III}_3 and Fe^{III}_4 clusters in the inter-domain iron binding cleft of *n*FbpA and *h*FbpA [9,31]. Hence, based on the structural evidence and the match of single-site binding model in ITC analysis supported by FTICR-ESI mass spectrometry data, it seems likely that all four Fe^{III} ions are bound as a cluster in the flexible interdomain cleft, where two tyrosines, a glutamate and a histidine side

chain are available for coordination. Binding of Fe^{III} at other sites might be expected to produce very different affinities and poor agreement with a single-site binding model.

ITC measures the total heat change upon addition of the titrant, and includes contributions from the heat of dilution of the titrant, deprotonation of the iron binding side chains, e.g. loss of protons from hydroxyl groups of Tyr195 and Tyr196, heat due to dissociation of citrate from iron(III), binding of citrate to *n*FbpA, and binding of iron(III) to the active site. In addition some of the iron citrate in the buffer (Tris pH 7.4) could be present as metal buffer adduct. Since the observed enthalpy change is for a series of events, this can clearly complicate the interpretation of the data. Since there is uptake of several iron(III) ions by the protein in these experiments, no attempt was made to deduce an effective binding constant taking into account the binding of each iron and its dissociation from citrate. In our experiments to saturate the protein with iron, ca. 10 mol equivalents of iron complex were added to the protein which resulted in the binding of ca. 4 Fe^{III}.

The apparent metal binding constant for all the titrations of Fe^{III} with wild type apo-*n*FbpA was ca. 10^5 M^{-1} (Table 2), which is close to the value reported previously for binding of a single iron to *n*FbpA using ITC [24]. The value of the apparent binding constant does not suggest very strong binding, but it is noted that the protein binds to Fe^{III} from a Fe^{III}-citrate complex, i.e. in competition with citrate, which is a strong chelator of Fe^{III}. Also the buffer contains Tris which itself has iron binding ability. Hence the binding may be stronger than the apparent binding constant appears to indicate. The x-ray crystal structures of Fe_3-FbpA and Fe_4-FbpA suggest that various modes of anchoring of Fe^{III} clusters to the tyrosine residues are possible and in these structures the histidine residue does not bind to the clusters [9,31]. Earlier work has shown that holo-*n*FbpA has a single iron bound [21]. The binding of a cluster might occur as a single event or as a series of one- or two-iron uptake processes whilst the binding cleft remains open. The ITC data can be fitted to a single-site binding model with no other steps, as observed for the binding of Fe^{III} in ovotransferrin [46], which suggests that binding of a preformed Fe^{III}_4 cluster

occurs effectively as a single event. Such a mechanism was proposed for the formation of Zr_3-Fbp [22].

Two models illustrating the possible cluster binding modes are shown in Chart 1. These models are consistent with the deconvoluted mass of 34375.2 Da for $[Fe_4O_2(OH)_4(H_2O)(cit)]^+$ bound to *n*FbpA. The mass spectrometric data suggest that the iron is bound to citrate in addition to protein side-chains and hence it is unlikely that the coordination environment of the four

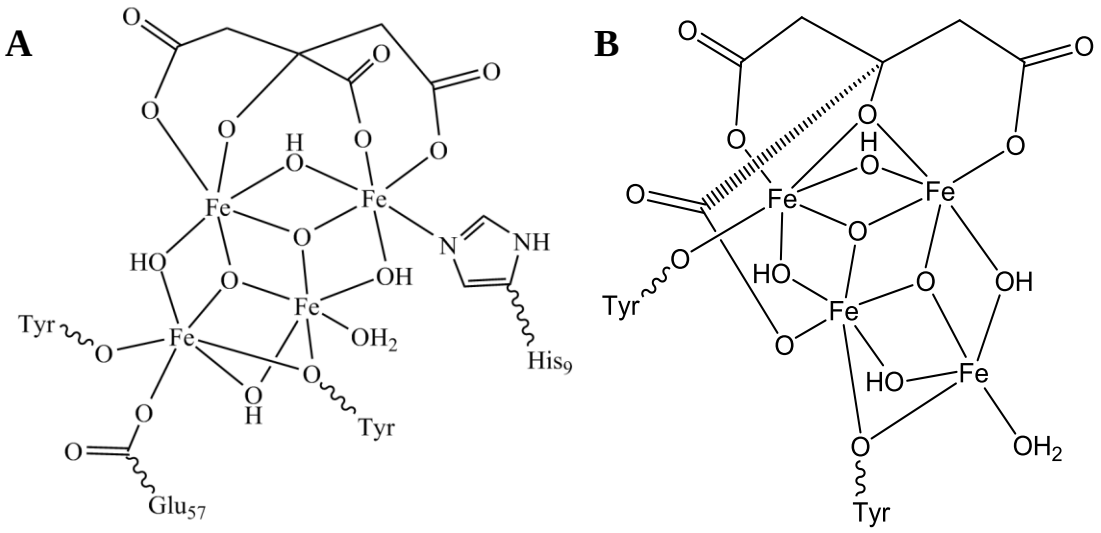

Chart 1 Proposed $[Fe_4O_2(OH)_4(H_2O)(C_6H_5O_7)]^+$ clusters (**A**) bound to the hydroxyl group of two tyrosines (Y_{195} and Y_{196}), an imine nitrogen of histidine (H_9) and the carboxylate group of glutamate (E_{57}) in *n*FbpA (**B**) bound to the hydroxyl group of two tyrosines (Y_{195} and Y_{196}) in *n*FbpA.

bound iron(III) ions is identical. Binding of the active site histidine to iron(III) may not involve deprotonation and the heat change involved may be too small to be detected by ITC. In the proposed model **A** the Fe^{III}_4 cluster is ligated by the Tyr, His and Glu protein side chains, by hydroxides, and by alkoxide and carboxylate groups of citrate, whereas in **B**, which is closer agreement with the structures containing bound clusters reported in literature, the Fe^{III}_4 cluster is ligated by the two tyrosines (Y_{195} and Y_{196}), by hydroxides, and alkoxide and carboxylate groups of citrate. The earlier reported Fe_3-*n*FbpA structure from one of our laboratories shows no binding of histidine (H_9) or glutamate (E_{57}) to the Fe_3-oxo(hydroxo) cluster [9]. It contains a

triangle of Fe^{III} ions with each pair bridged by a μ_2-oxygen. A central μ_3-oxygen is co-ordinated to all the three Fe^{III} ions. Three additional terminal oxygens co-ordinate to each Fe^{III} of the tightly bridged Fe_3O_4 unit and complete the oxygen co-ordination shell of the octahedral iron atoms within the Fe_3O_{13} cluster [9]. Our postulated Fe_4-*n*FbpA models are in good agreement with the above except that the bonding to H_9 and E_{57} in model **A** is absent in the structures reported in literature. These models contain two Fe_3-triangles with a common edge and two central μ_3-oxygen which each co-ordinate to three Fe atoms. In addition each Fe pair is bridged by a μ_2-oxygen from hydroxyl groups. The binding of a tyrosine phenolate oxygen to two Fe^{III} centers is also consistent with our earlier report in which we found that the tyrosine may bind in various ways and to up to three Fe^{III} ions [9]. The binding to H_9 and E_{57} is proposed to satisfy the expected six co-ordination iron(III) in the modeled species including a binding mode for citrate which is prevalent at pH ~7.4 [47]. However based on the reported crystal structures, the bonds to H_9 and E_{57} might not be present. If so, then model **B** in Chart 1 is consistent with the literature.

One of the iron(III) ions in model **B** may be five co-ordinate as found for the fourth iron in the reported Fe_4-N175L-*h*FbpA structure [10]. Shouldice *et al.* reported two structures of *h*FbpA variants with Fe_3 and Fe_4 clusters. The Fe_3-H9A-*h*FbpA structure contains two phosphate anions, one of which binds to all the three ferric/ferrous ions and the other to two of the ferric/ferrous ions and each metal is coordinated by six oxygens, the shortest coordination distances being for the tyrosine phenolate oxygens, which are strongly bound [10]. Since there is a H9A mutation there is no possibility of histidine binding. However, the Fe_4-N175L-*h*FbpA also do not show any Fe-N bond involving the histidine. However, this mutation of N175 may affect the cleft structure and histidine binding [10]. Fe_4-N175L-*h*FbpA has only one phosphate bound to three ferric/ferrous ions and the fourth iron points towards a vacant site which is occupied by phosphate in the Fe_3-H9A-*h*FbpA structure [10]. In our model, three of the Fe^{III} ions are six co-ordinate with oxygen coordination, in good agreement with the reported iron clusters in FbpA discussed above [9,10]. A major difference in our models arises from the use of citrate as an

anion rather than phosphate as was reported for the Fe_3 and Fe_4 clusters in FbpA variants. The coordination mode for citrate in the model is consistent with that found for iron in citrate compounds reported in literature [47-49].

ICP-MS experiments suggested that some of the bound iron is readily removed. Buffer exchange for ammonium acetate reduced the metal content of the protein by ~50% after 3 exchanges with 20 mM NH_4OAc, from ca. 4.25 Fe to 1.8 Fe for *n*FbpA and to 2.2 Fe^{III} per protein for H9Y-*n*FbpA, consistent with the binding of an Fe_4-cluster in an open cleft such that some bound iron is readily accessible to competing ligands. The concentration of the Fe_4^{III}-*n*FbpA is more than 200-fold lower than the concentration of ammonium acetate and for each exchange of buffer there is competition with a large excess of acetate for iron binding. The extraction of iron from the protein is presumably due to competition from the large excess of acetate used (200x).

The calorimetric titrations of *wild type* apo-*n*FbpA and apo-H9Y-*n*FbpA carried out in 50 mM Hepes buffer at pH 7.4 shows that the presence of Hepes buffer shows a ca. 7-fold decrease in the apparent binding constant (K_{app}^{ITC}) for wild type and a 2-fold decrease for the mutant H9Y-*n*FbpA (Table 2) when compared to the binding in Tris buffer. The binding enthalpies are also considerably lower (Table 2). The stoichiometry for iron binding is still $4Fe^{III}$ per *n*FbpA however the K_{app}^{ITC} was 8.4(6) x 10^4 M^{-1} and ΔH (-0.30(7) kcal mol^{-1}) (Fig. S1). Under similar conditions apo-H9Y-*n*FbpA binds 4.18(3) Fe^{III} per protein (Fig. S2), and again the K_{app}^{ITC} (4.5(5) x 10^5 M^{-1}) and ΔH (-0.48(5) kcal mol^{-1}) are lower than in Tris buffer. The origin of this effect may be due to the speciation of iron citrate in the two buffers. In Hepes, which coordinates to Fe^{III} only weakly, very stable iron citrate polymers may form making the iron less available for binding to Fbp. In Tris, which can bind more strongly to Fe^{III}, the citrate polymers may be broken down into smaller clusters which can more readily bind in the cleft of the protein.

For some pathogenic bacteria, the iron binding site in FbpA contains three tyrosines [28,29]. Hence, we studied the mutant H9Y-*n*FbpA to determine how replacement of the binding site

histidine by a third tyrosine would influence Fe^{III} binding. ITC binding experiments with ferric ammonium citrate showed that the integrated heat of binding for H9Y-*n*FbpA (-1.03(6) kcal mol^{-1}) is similar to that for wild type *n*FbpA (-0.95(5) kcal mol^{-1}). This implies that the new tyrosine-9 residue may not be involved in metal binding. However, the mutant protein has a higher affinity the Fe_4 cluster, the binding constant increasing by two fold to 1.1(7) x 10^6 M^{-1} (Table 2). The ESI mass spectrometric analysis of this Fe_4-H9Y-*n*FbpA suggests that the protein does not have a high affinity for citrate as the synergistic anion, citrate is more readily lost in ESI MS experiments compared to native *n*FbpA. However the iron ions remain bound even in the gas phase. The deconvolution of the mass spectrometric data gives a mass of 34443.0 Da consistent with the composition [H9Y-*n*FbpA-$Fe_4O_2(OH)_4$(cit)$(H_2O)_4$ + (cit) + $2H^+$]$^{12+}$ (Calc. 34438.9 Da; Figure S4). The most abundant species found in the mass spectrum matches well with [H9Y-*n*FbpA-$Fe_4O_2(OH)_4(H_2O)$ + $2H^+$]$^{12+}$ 34008.0 (Calc. 34007.8) Da.

Since we found that in gas phase even in the absence of citrate an Fe_4 cluster was bound to H9Y-*n*FbpA, we investigated the binding of iron to the protein in absence of citrate using 9 mol equiv of $^{57}FeCl_3$ in Tris at pH 7.4. The FTICR-ESI-MS results suggested the presence of an Fe^{III}_4 cluster with a monoisotopic mass of 34062.7 Da consistent with [H9Y-*n*FbpA-$^{57}Fe_4O_2(OH)_4(H_2O)_3Na]^{12+}$ (Fig. 7).

Since *n*FbpA appeared to bind readily a tetranuclear iron cluster, we investigated whether such iron binding could occur inside cells. ^{57}Fe-citrate was added to a culture medium containing TOP10 *E. coli* cells with the plasmid DNA of *n*FbpA. A control culture of the same *E. coli* cells without *n*FbpA DNA was also studied. The *E. coli* cell pellets without any *n*FbpA present were EPR silent, but gave a reasonable Mössbauer signal. The simulation of the Mössbauer data **(**Fig. 8) by means of the spin-Hamiltonian formalism [41,42] (solid lines in Fig. 8**)** showed good agreement with the experimental data. However it should be noted that the model used for reproducing the experimental spectra is a pure fit model and the parameters given in Table 3

have no deeper meaning. Nevertheless this model can be used to analyze the spectra from *E. coli* cells containing *n*FbpA.

The Mössbauer spectra of the *E. coli* cells containing *n*FbpA are displayed in Figs. 9 and 10. The simulation of the experimental data obtained at high fields (Fig. 10) using the spin-Hamiltonian formalism indicates the presence of a diamagnetic Fe^{III} species (~7%), which may be a dinuclear high-spin Fe^{III} species with the spins of the ferric ions antiferromagnetically coupled. The strong antiferromagnetic spin coupling in the Fe^{III} dinuclear species leads to diamagnetism which is quite similar to the coupling observed for dimeric oxygen-bridged Fe^{III} centers in methane monooxygenase [43]. Also a significant amount of polynuclear ferric high-spin species (~27%) was present, for which the Mössbauer signal splits into two components at higher fields. Such a behavior is consistent with the presence of iron-clusters of higher nuclearity inside the *n*FbpA expressing *E. coli* cells. Since a Mössbauer signal for the oligomeric iron species is not observed in the *E. coli* cells without *n*FbpA, it seems likely that the Mössbauer signal for the oligomeric iron species (Fe_n, $n \geq 4$) may arise $^{57}Fe_n$-*n*FbpA.

This leads to the hypothesis that the iron-binding ability of *n*FbpA might not be the same inside the cells and *in vitro*. The protein might even contain dinuclear and polynuclear iron species when inside cells displaying a heterogeneous behaviour. The cellular environment would have phosphate also present which could compete with citrate and that might lead to different speciation in terms of nuclearity and synergistic anion. It is remarkable to find that in iron-rich environments the protein does have a tendency to bind to multiple iron clusters even inside *E. coli* cells as observed in the Mössbauer spectroscopic experiments. Thus the Mössbauer spectroscopic data complements our findings for Fe_4-*n*FbpA and Fe_4-H9Y-*n*FbpA using mass spectrometry and ITC by revealing multiple irons bound to *n*FbpA inside *E. coli* cells. However, when the ^{57}Fe enriched protein was extracted from the *E. coli* cells using a reported purification procedure [40], the extracted protein did not show the presence of any polynuclear iron clusters; only a single Fe^{III} containing *n*FbpA was observed by Mössbauer spectroscopy. This may be due

to the fact that the extraction of the protein is carried out in presence of a detergent, cetyl trimethylammonium bromide, and then binding the protein to a resin and extracting through elution with increasing concentration of NaCl. Such harsh treatment to extract the protein from the cell may be sufficient to remove the relatively labile polynuclear iron species leaving only a single iron bound ^{57}Fe-*n*FbpA. Our ICP-MS data also suggest that some of the bound iron is readily removed during sample preparation for ICP-MS. This again suggests that the binding of an Fe_4 cluster and a citrate prevents the Venus-fly-trap cleft of *n*FbpA from closing rendering some of the iron labile through being relatively easily accessible. How much iron dissociates depends the nature of the treatment.

Studies of a single iron binding to *n*FbpA by ITC in the presence and absence of phosphate using 3.5 mM $FeCl_3$ and 30 mM citrate at pH 7.0 have been reported [24]. These gave a binding constant for Fe^{III}-*n*FbpA in absence of phosphate of 1.6 x 10^4 M^{-1}. Our ITC data for iron binding to apo-*n*FbpA using 4 mM citrate suggests that four iron ions bind to the protein. The major differences between the two experiments are the concentration of citrate which is ca. 7 times lower in our experiments, and the higher ratio of iron-to-protein FbpA:Fe (1:50) used in our studies compared to 1:25 in the literature report. Comparing our studies with those of Murphy et al. [24] suggests that when other iron chelators such as citrate are lower in concentration and the iron(III) concentration is high, then the protein can bind multiple iron atoms in the interdomain binding cleft with an apparent binding constant 7.6 x 10^4 M^{-1} and ΔH = -0.87 kcal mol^{-1} at pH 7.4 (vs. 1.6 x 10^4 M^{-1}, ΔH = -0.46 kcal mol^{-1}, pH 7.0 in literature) [24]. Hence this suggests that although the protein has a higher affinity for iron compared to citrate, at sufficiently high citrate concentrations iron uptake by the protein can be inhibited. This co-relates well with the use of citrate to remove iron from the protein at pH 6.0 as mentioned in the materials and methods section. Further increase in the value of K_{app}^{ITC} in absence of pre-equilibrated citrate (6.0(5) x 10^5 M^{-1}) supports the above statement. In addition citrate might as well be accommodated in the inter domain binding cleft even in absence of iron(III), and hence for the iron(III) to bind to the

protein, the pre-bound citrate has to be displaced from the binding cleft. This is reflected in the initial slope of the binding isotherm in the titration of iron-citrate with citrate pre-equilibrated FbpA (Fig. 4), but could not be fitted quantitatively.

There is a two-fold increase in affinity for an Fe^{III} cluster of the mutant H9Y-*n*FbpA containing three tyrosines in the cleft compared to the wild-type protein. This may be indicative of a role for the extra Tyr residue in the FbpA of several organisms, such as *Campylobacter jejuni* and *Bordetella pertussis*. However, it is evident that when complex equilibria are involved in metal binding, subtle changes in the binding site may not be reflected in the binding enthalpy especially in buffer media where there is multiple speciation of iron(III). However, the ITC and mass spectrometry studies strongly suggest that tetranuclear iron(III)-oxo clusters bind in the 'Venus fly-trap' cleft. Although we could not dissect all the steps in the binding of metal to protein, the studies provided information on the apparent binding constant (in the presence of competitive binding by citrate, a strong chelator of Fe^{III}), the overall enthalpy of reaction and stoichiometry of the multiple metal binding to *n*FbpA.

Mössbauer spectroscopic studies of *n*FbpA in *E. coli* cells indicated the presence of polynuclear high-spin Fe^{III} species, suggesting that the protein can bind iron clusters *in vivo* in iron-rich environments. Future work will explore the mechanism of iron binding to FbpA using a range of biophysical techniques. We aim to understand how the apo-FbpA protein closes around its iron target in the periplasm and to further identify and capture any intermediate complexes to shed light on this fundamental process.

Acknowledgements

We thank European Commission for a Marie Curie Fellowship for AM, the BBSRC (RASOR, IRColl in Proteomic Technologies), EPSRC (WCAS), AWM/ERDF (Science City) and ERC (Grant no. 247450, BIOINCMED) for funding, the Universities of Edinburgh and Warwick for analytical facilities, and Dr Teresa Pinheiro for access to isothermal calorimetry. AM thanks

IISER Kolkata for financial support. VS acknowledges the federal state Rheinland-Pfalz of Germany for financial support within the framework of NANOKAT.

References

[1] Sutak R, Lesuisse E, Tachezy J, Richardson DR (2008) Trends Microbiol 16:261-268.

[2] Nyilasi I, Papp T, Takó M, Nagy E, Vágvölgyi C (2005) Acta Microbiol Immunol Hung 52:185-97.

[3] Mietzner TA, Tencza SB, Adhikari P, Vaughan KG, Nowalk AJ (1998) Curr Top Microbiol Immunol 225:113-35.

[4] Sun H, Li H, Sadler PJ (1999) Chem. Rev. 99:2817-2842.

[5] Weaver KD, Gabricevic M, Anderson DS, Adhikari P, Mietzner, TA, Crumbliss, AL (2010) Biochem 49:6021-6032.

[6] Guo M, Harvey I, Campopiano DJ, Sadler PJ (2006) Angew Chem Int Ed Engl 45:2758-2761.

[7] Zhong W, Alexeev D, Harvey I, Guo M, Hunter DJ, Zhu H, Campopiano DJ, Sadler PJ (2004) Angew Chem Int Ed 43:5914-5918.

[8] Alexeev D, Zhu H, Guo M, Zhong W, Hunter DJ, Yang W, Campopiano DJ, Sadler PJ (2003) Nat Struct Biol 10:297-302.

[9] Zhu H, Alexeev D, Hunter DJ, Campopiano DJ, Sadler PJ (2003) Biochem J 376:35-41.

[10] Shouldice SR, Skene RJ, Dougan DR, McRee DE, Tari LW, Schryvers AB (2003) Biochemistry 42:11908-11914.

[11] Lippard SJ (2005) Phil Trans R Soc A 363:861-877.

[12] Decker A, Clay MD, Solomon EI (2006) J Inorg Biochem 100:697-706.

[13] Vignais PM, Billoud B (2007) Chem Rev 107:4206-72.

[14] Liu J, Lou Y, Yokota H, Adams PD, Kim R, Kim SH (2005) J Biol Chem 280:15960-15966.

[15] Lill R, Mühlenhoff U (2008) Annu Rev Biochem 77:669-700.

[16] Fontecave M, Ollagnier-de-Choudens S (2008) Arch Biochem Biophys 474:226-237.

[17] Kovaleva EG, Neibergall MB, Chakrabarty S, Lipscomb JD (2007) Acc Chem Res 40:475-483.

[18] Dhungana S, Anderson DS, Mietzner TA, Crumbliss AL (2004) J Inorg Biochem 98:1975-1977.

[19] Zhu H, Alexeev D, Hunter DJ, Campopiano DJ, Sadler PJ (2003) Biochem J 376:35-41.

[20] McRee DE, Bruns CM, Williams PA, Mietzner TA, Nunn R Research Collaboratory for Structural Bioinformatics protein Data Bank (RCSB PDB). DOI:10.2210/pdb1d9y/pdb

[21] Alexeev D, Zhu H, Guo M, Zhong W, Hunter DJB, Yang W, Campopiano DJ, Sadler PJ (2003) Nat Struct Biol 10:297-302.

[22] Zhong W, Alexeev D, Harvey I, Guo M, Hunter DJB, Zhu H, Campopiano DJ, Sadler PJ (2004) Angew Chem Int Ed 43:5914-5918.

[23] Nowalk AJ, Vaughan KG, Day BW, Tencza SB, Mietzner TA (1997) Biochemistry 36:13054-13059.

[24] Bekker EG, Creagh AL, Sanaie N, Yumoto F, Lau GHY, Tanokura M, Haynes CA, Murphy MEP (2004) Biochemistry 43:9195-9203.

[25] Shouldice SR, Skene RJ, Dougan DR, Snell G, McRee DE, Schryvers AB, Tari LW (2004) J Bacteriol 186:3903-3910.

[26] Shouldice SR, Dougan DR, Williams PA, Skene RJ, Snell G, Scheibe D, Kirby S, Hosfield DJ, McRee DE, Schryvers AB, Tari LW (2003) J Biol Chem 278:41093-41098.

[27] Shouldice SR, McRee DE, Dougan DR, Tari LW, Schryvers AB (2005) J Biol Chem 280:5820-5827.

[28] Tom-Yew SAL, Cui DT, Bekker EG, Murphy MEP (2005) J Biol Chem 280: 9283-9290.

[29] Tom-Yew SAL, Shilton BH, Bekker EG, Tocheva EI, Murphy MEP. Research Collaboratory for Structural Bioinformatics protein Data Bank (RCSB PDB). DOI:10.2210/pdb2owt/pdb.

[30] Bruns CM, Anderson, DS, Vaughan KG, Williams PA, Nowalk AJ, McRee DE, Mietzner TA (2001) Biochemistry 40:15631-15637.

[31] Bruns CM, Nowalk AJ, Arvai AS, McTigue MA, Vaughan KG, Mietzner TA, McRee DE (1997) Nat Struct Biol 4:919-924.

[32] Shouldice SR, Dougan DR, Skene RJ, Tari LW, McRee DE, Yu R-H, Schryvers AB (2003) J Biol Chem 278:11513-11519.

[33] Khan AG, Shouldice SR, Tari LW, Schryvers AB (2007) Biochem J 403:43-48.

[34] Khan AG, Shouldice SR, Kirby SD, Yu RH, Tari LW, Schryvers AB (2007) Biochem J 404:217-225.

[35] Benda R, Tse Sum Bui B, Schunemann V, Florentin D, Marquet A, Trautwein AX (2002) Biochemistry 41:15000-15006.

[36] Matzapetakis M, Raptopoulou CP, Tsohos A, Papaefthymiou V, Moon A, Salifoglou A (1998) J Am Chem Soc 120:13266-13267.

[37] Guo M, Harvey I, Yang W, Coghill L, Campopiano DJ, Parkinson JA, MacGillivray RT, Harris WR, Sadler PJ (2003) J Biol Chem 278:2490-2502.

[38] Pace CN, Vajdos F, Fee L, Grimsley G, Gray T (1995) Protein Sci. 4:2411-2423.

[39] Ferreirós C, Criado MT, Gómez JA (1999) *Comparative Biochemistry and Physiology B.* 123:1–7.

[40] Dhungana S, Taboy CH, Anderson DS, Vaughan KG, Aisen P, Mietzner TA, Crumbliss AL (2003) Proc Natl Acad Sci USA 100:3659-3664.

[41] Schünemann V, Winkler H (2000) Rep Prog Phys 63: 263-353.

[42] V. Schünemann und H. Paulsen (2007) Mössbauer Spectroscopy, in Application of Physical Methods to Inorganic and Bioinorganic Chemistry, edited by Robert A. Scott and Charles M. Lukehart, John Wiley and Sons, Ltd., ISBN: 978-0-470-03217.

[43] Fox B-G, Hendrich M-P, Surerus K-K, Andersson K-K, Froland W-A, Libscomb J-D, Münck E (1993) J. Am. Chem. Soc. 115:3688 – 3701.

[44] Lynch J-B, Juarez-Garcia C, Münck E, Que L Jr (1989) J. Biol. Chem. 264:8091 – 8096.

[45] Tse Sum Bui B, Benda R, Schünemann V, Florentin D, Trautwein AX, Marquet A (2003) Biochemistry 42:8791-8798.

[46] Lin L-N, Mason AB, Woodworth RC, Brandts JF (1991) Biochemistry 30**:**11660-1 1669.

[47] Gautier-Luneau I, Merle C, Phanon D, Lebrun C, Biaso F, Serratrice G, Pierre J-L (2005) Chem. Eur. J. 11:2207-2219.

[48] Shweky I, Bino A, Goldberg DP, Lippard SJ (1994) Inorg. Chem. 33:5161-5162.

[49] Liu J-Q, Wang Y-Y, Ma L-F, Zhang W-H, Zeng X-R, Zhong F, Shi Q-Z, Peng S-M (2008) Inorg.Chim.Acta 361:173-182.